Osteoarthritis and Cartilage 28 (2020) 1559–1571

Osteoarthritis and Cartilage

Endothelin-1 induces chondrocyte senescence and cartilage damage via endothelin receptor type B in a post-traumatic osteoarthritis mouse model

M. Au † [a], Z. Liu † ‡ [a], L. Rong ‡, Y. Zheng †, C. Wen † [*]

† Department of Biomedical Engineering, Faculty of Engineering, Hong Kong Polytechnic University, Kowloon, Hong Kong
‡ Department of Spine Surgery, The Third Affiliated Hospital of Sun Yat-Sen University, China

ARTICLE INFO

Article history:
Received 8 March 2020
Accepted 14 August 2020

Keywords:
Osteoarthritis
Endothelin-1
Endothelin type B receptor
Reactive oxygen species
Senescence

SUMMARY

Objectives: This study aimed to investigate the role of endothelin-1 (ET-1), originally known as the potent vasoconstrictor, and its receptors in chondrocyte senescence and osteoarthritis (OA) development.

Method: Temporal changes of ET-1 and its receptors with OA development were characterized in a posttraumatic OA (PTOA) mouse model at time zero, 1-month and 4-month after surgical induction via destabilization of medial meniscus (DMM). A transgenic ET-1 overexpression (TET-1) mouse model was deployed to assess the impact of upregulated ET-1 on chondrocyte senescence and cartilage degradation. Effects of endothelin receptor blockade on chondrocyte senescence and OA development were further examined both *in vitro* and *in vivo*.

Results: Local expression of ET-1 in subchondral bone and synovium upregulated after DMM with an increase of plasma ET-1 level from 3.18 ± 0.21 pg/ml at time zero to 6.47 ± 0.34 pg/ml at 4-month post-surgery. Meanwhile, endothelin type B receptor (ET_BR) (53.31 ± 2.42% to 83.8 ± 2.65%) and $p16^{INK4a}$ (10.91 ± 1.07% to 28.2 ± 1.0%) positve chondrocytes accumulated in articular cartilage since 1-month prior to cartilage loss at 4-month post-surgery. Overexpressed ET-1 promoted $p16^{INK4a}$-positive senescent chondrocytes accumulation and cartilage degradation in TET-1 mice. Selective blockade of ET_BR, but not ET_AR, lowered the expression of $p16^{INK4a}$ in ET-1 or H_2O_2-induced chondrocyte senescence model, and mitigated the severity of murine PTOA. Intriguingly, reactive oxygen species (ROS) scavenger, Vitamin C, could rescue ET-1-induced chondrocyte senescence *in vitro* associated with restoration of mitochondrial dynamics.

Conclusion: ET-1 could induce chondrocytes senescence and cartilage damages via ET_BR in PTOA.

Introduction

Osteoarthritis (OA) is one of the most common causes of disability in adults[1]. The hallmark of OA is cartilage degradation. In human OA cartilage lesions, senescent cells are detected near the cluster of chondrocytes[2]. Adult articular chondrocytes have limited proliferation capacity. In response to altered mechanical loading[3,4] or oxidative stress[5], articular chondrocytes undergo premature senescence with shortening of telomeres, which provokes the onset of OA[6]. Overexpressed senescence marker $p16^{INK4a}$ was sufficient to induce production of two major cartilaginous matrix remodelling enzymes: matrix metalloproteinase (MMP)-1 and -13[7]. Targeted ablation of $p16^{INK4a}$-positive senescent chondrocytes (SnCs) could mitigate OA in genetically modified mice[6]. Collectively, SnCs are the emerging therapeutic targets for OA[20].

Vascular aetiology of OA has been proposed for decades[8]. Increased newly-formed blood vessels were found in OA synovium and osteochondral junction in both human and rodents[9]. Our previous studies have demonstrated the association of endothelial dysfunction in synovium and subchondral bone with articular cartilage damage in murine PTOA[10,11]. Yet the underlying molecular mechanism remains poorly understood.

Endothelin-1 (ET-1), the most potent vasoconstrictor predominantly expressed in endothelium, plays a pivotal role in vascular

* Address correspondence and reprint requests to: C. Wen, Department of Biomedical Engineering, Faculty of Engineering, The Hong Kong Polytechnic University, Hong Kong, Tel: 852-34008898; Fax: 852-23342429.
E-mail addresses: 15903037R@connect.polyu.edu (M. Au), liuzhongyu8731@163.com (Z. Liu), ronglimin@21cn.com (L. Rong), chunyi.wen@polyu.edu.hk, yongping.zheng@polyu.edu.hk (C. Wen).
[a] Equal contribution.

https://doi.org/10.1016/j.joca.2020.08.006
1063-4584/

tone maintenance and a plethora of age-related pathologies including OA[12,13]. ET-1 transduces its biological functions through transduction via two G protein-coupled receptors, endothelin type A receptor (ET_AR) and type B receptor (ET_BR). ET-1 has been recently shown to promote formation of ROS and induce cellular senescence while blocking ET_BR lowered ET-1-induced ROS and senescent cells accumulation in endothelium[14,15]. Meanwhile, serum and synovial fluid ET-1 was found to associate with the severity of radiographic knee OA in human[16]. Moreover, ET-1 induces NFκB activation in a variety of cells such as macrophages and chondrocytes[17]; ET_AR or ET_BR antagonism attenuates NFκB activation and mitigates senescence-associated secretory phenotypes (SASPs) including MMP-13 *in vitro*[18,19].

Collectively, we hypothesize that ET-1 leads to chondrocyte senescence and cartilage damage through its receptors. We will test this hypothesis with the following aims 1) to characterize the spatiotemporal changes of local and systemic ET-1 with OA development in a DMM-induced PTOA mouse model; 2) to evaluate the effect of ET-1 overexpression or endothelin receptor blockade on chondrocyte senescence and cartilage degradation in murine PTOA; 3) to investigate the underlying molecular mechanism of ET-1-induced chondrocyte senescence.

Method

Institutional Animal Subjects Ethics Sub-Committee (ASESC) approved all the experiments listed below (ASESC Case # 15–16/29-BME-R-GRF).

DMM-induced PTOA mouse model

Animals were raised in constant temperature at 25°C, with 12/12 light–dark cycle and supplied with food and water ad libitum. To generate a post-traumatic OA model, destabilization of medial meniscus (DMM) surgery was performed on 6-month old balb/c male mice according to an established protocol[20]. Briefly, mice were put in general anaesthesia by intraperitoneal injection of an anaesthetic cocktail [ketamine (100 mg/ml): Xylazine (20 mg/ml): saline = 1:0.5:8.5]. The medial meniscus was destabilized under general anaesthesia. Animals were allowed to recover on a heating pad until they are fully recovered from the anaesthetics. Drug treatment started one day after the surgery. Sample size estimation was performed based on the difference in Osteoarthritis Research Society International (OARSI) histopathological score between the control and endothelin receptor antagonist treatment group as previously reported[21]. Assuming a pooled standard deviation of 8 units, the study would require a sample size of 7 for each group to achieve a power of 80% and a level of significance of 5% (two sided), for detecting a 12.25-unit difference in the means between surgery and treatment group using two-sample independent *t* test. *To allow for 10% ineligibility, 8 mice were used in each group.* Animals were randomly divided into 7 groups: a baseline group without DMM surgery ($n = 4$); 1-month ($n = 8$) and 4-month ($n = 7$) post-DMM groups with vehicle injection; 1-month ($n = 8$) and 4-month ($n = 8$) post-DMM with 1 mg/kg BQ123 (a selective ET_AR blocker) (Sigma, USA) treatment; 1-month ($n = 8$) and 4-month ($n = 7$) post-DMM with 1 mg/kg BQ788 (a selective ET_BR blocker) (Sigma, USA) treatment. Vehicles and drugs were administered intraperitoneally on a daily basis. Two mice died due to unexpected general anaesthesia accident during imaging examination, therefore were excluded in the analysis.

Transgenic ET-1 overexpression mouse model

Transgenic mice overexpressing ET-1 in endothelial cells (TET-1) were given as a gift from Prof. Sookja Kim CHUNG form the University of Hong Kong. The transgenic mouse model was generated by microinjection of ET-1 construct, which contains mouse ET-1 cDNA with SV40 polyA driven by Tie-1 promoter. Genotyping was carried out to confirm the homogeneity of the animals used in the study (Fig. S1). Five TET-1 and four wildtype from the same litter at the age of 9-month were used in this experiment.

Evaluation of OA severity using multiple imaging modalities

Vascular volume and function measurement by power doppler (PD) and photoacoustic (PA) imaging

The vascular volume from PA (PAVV) and PD (PDVV) imaging as well as the tissue oxygenation level (sO_2) were measured using Vevo2100 high-frequency Micro-Imaging System (VisualSonics, Canada) in order to evaluate angiogenesis, vessel function as well as oxygenated haemoglobin in synovium respectively[11]. PD images were acquired using 50 MHz ultrasound transducer with a bandwidth of 30–70 MHz (MS700), while PA images were acquired using 30 MHz ultrasound transducer with a bandwidth of 18–38 MHz (LZ400). Briefly, a tendon–tibia–femur (TTF) triangle in murine knee joint was defined as the region of interest (ROI) in 2D ultrasonic and PA images. The vascular volume (%) was measured by linear translocation of the transducer perpendicular to the sagittal plane of the 2D image, and then calculated by multiplying the number of colour pixels by 0.032 mm (slice thickness) and divided by total number of voxels in volume of interest.

Microstructure analysis of tibia subchondral bone using microcomputed tomography (μCT)

Knees were scanned using Viva CT40 (Scanco, Switzerland) and analysed by a built-in software. Isotropic voxel size for the scan was 10.5 μm. X-Ray voltage and filter used were 70 kV and 1.0 respectively. Bone volume over total volume (BV/TV), trabecular number (Tb. N.) and trabecular thickness (Tb. Th.) were generated from the ROI in the subchondral bone of tibia.

Measurement of plasma ET-1 level

Endothelin-1 ELISA kit (Abcam, UK) was used to quantify endothelin-1 in plasma of mice according to the manufacturer's protocol. Blood was withdrawn from the animal on the day of sacrifice. Plasma was obtained by centrifuging blood at 1,600×*g* for 15 min at 0° C. The concentration of ET-1 was determined by the assay. Results were expressed as mean ± SEM of plasma samples.

Histological/immunohistochemical evaluation of OA knee joints

Samples were fixed and embedded following standard protocols. Samples were cut into 5 μm sections using microtome. Sections were stained with haematoxylin and eosin (H&E) and Safranin O/Fast green according to standard staining protocols for evaluation of histomorphology of the knee sections. Severity of OA was graded by a modified OARSI score (cartilage)[22,23] (Fig. S2) by two independent observers (one carried out blinded assessment). The agreement between the data obtained by observers was assessed by Cohen's kappa coefficient using online calculator QuickCals from Graphpad. The average scores from two independent observers were obtained for analysis. ImageJ was used to measure the thickness of hyaline cartilage (HC). All H&E and Safranin O images were taken using Nikon Eclipse 80i Microscope (Nikon, Japan).

Immunohistochemical staining was performed to detect specific proteins in our samples. Antigen retrieval and quenching of endogenous peroxidase activity were performed. After blocking, primary antibodies were incubated with the samples at 4°C overnight. Primary antibodies used: Endothelin 1 (1:2000; Abcam,

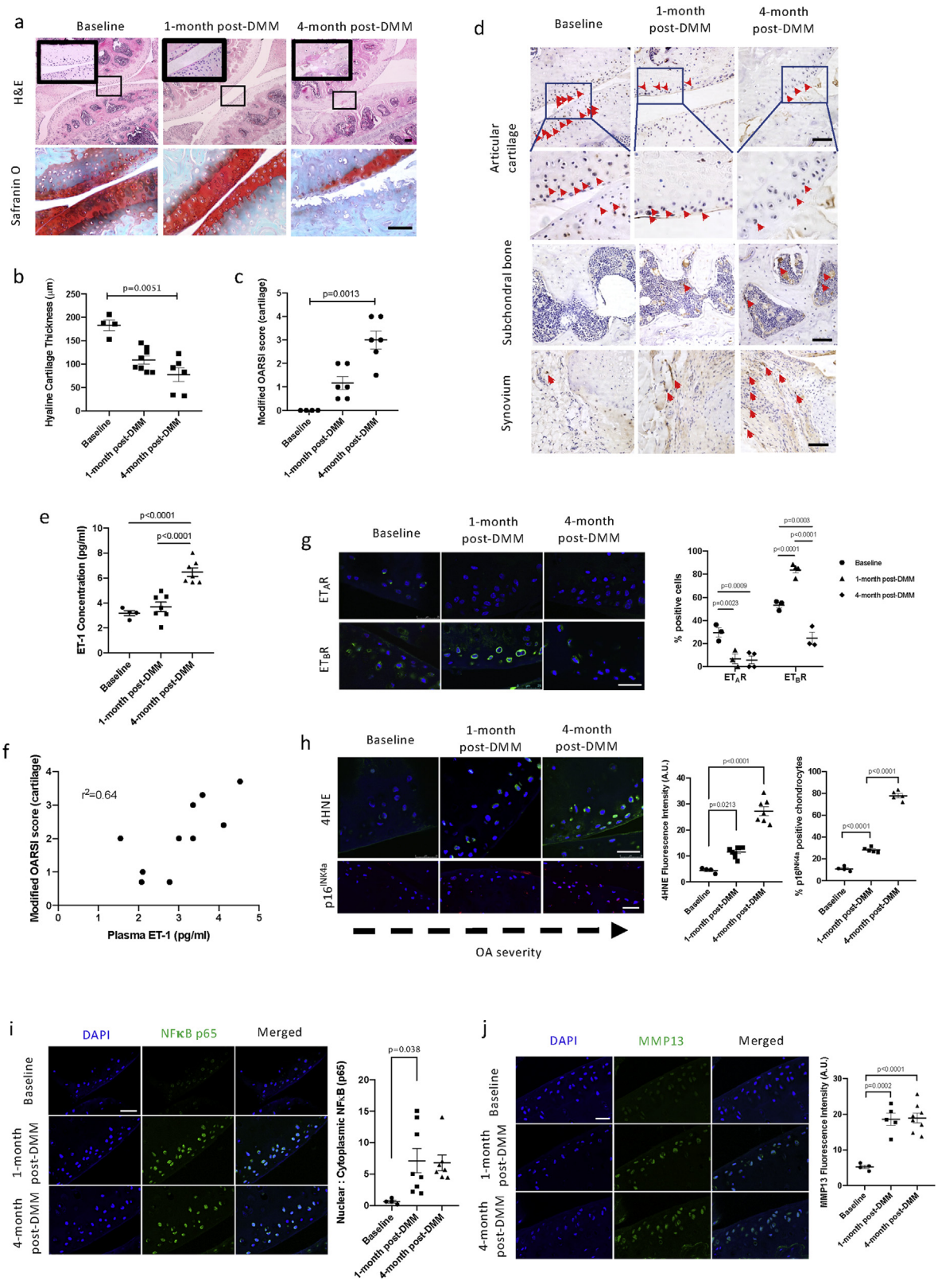

Fig. 1

ET-1, its receptors and proteins expression along DMM-induced post-traumatic OA development. (a) Representative images of H&E and safranin O/Fast green staining from baseline (***n*** = 4), 1-month post-DMM (***n*** = 8) and 4-month post-DMM (***n*** = 7) mice. Inlets depict close-up views of articular surface. Scale bar, 100 μm. (b) Thickness of hyaline cartilage along with PTOA progression. (c) Modified OARSI score (cartilage) score for baseline, 1-month post-DMM and 4-month post-DMM mice. (d) Representative images of immunostaining for ET-1 (brown, red arrows). Enlarged images show close-up views of articular surface.

Osteoarthritis and Cartilage

Scale bar, 100 μm. (e) Plasma ET-1 concentration in baseline, 1-month post-DMM and 4-month post-DMM mice. (f) Relationship between modified OARSI score (cartilage) and plasma ET-1 level. A moderate positive correlation was shown ($r^2 = 0.6440$, $\boldsymbol{n} = 10$). (g–h) Representative images of immunofluorescence staining and quantification of (g) endothelin receptors, ET_AR (green), ET_BR (green) and (h) 4HNE (green) and $p16^{INK4a}$ (red) on articular cartilage for baseline, 1-month post-DMM and 4-month post-DMM group with DAPI (blue) for nuclear identification. Scale bar, 25 μm. (i–j) Representative images of immunofluorescence staining and quantification of (i) NFκB p65 (green) and (j) MMP13 (green) on articular cartilage from each group with DAPI (blue) for nuclear identification. Scale bar, 25 μm All data are expressed as means ± SEM, and each data point represents an individual mouse. Ordinary one-way ANOVA or Kruskal–Wallis test was used to compare differences between groups when deemed appropriate, respective post-hoc tests were carried when overall significance was detected between groups.

ab117757), Endothelin type A Receptor (1:2000; Abcam, ab117521), Endothelin type B Receptor (1:2000; Abcam, ab117529), CDKN2A/$p16^{INK4a}$ (1:1000; Abcam, ab211542), NFκB p65 (1:500; Abcam, ab16502), 4-Hydroxynonenal (4HNE) antibody (1:50; Abcam, ab46545) and MMP13 antibody (1:200; Abcam, ab39012). For 3,3'-diaminobenzidine (DAB) staining, Vectastain ABC kit and DAB substrate kit for peroxidase (Vector Labs, USA) were used to stain targeted antigens followed by counterstaining using Harris Haematoxylin. For fluorescence staining, visualization of positive signals was performed using Donkey anti-Rabbit IgG H&L (DyLight® 488), Goat anti-Mouse IgG (H + L) (Alexa Fluor® 488) and Goat anti-Mouse IgG (H + L) Superclonal™ (Alexa Fluor® 647) secondary antibodies. The negative immune controls underwent the same procedure without primary antibody. Quantification using percentage of positive cells or fluorescence intensity was performed when deemed appropriate. Images were taken using Leica TCS SPE Confocal Microscope at a magnification of 200×.

Chondrocyte senescence model using ATDC5

ATDC5 cell line was received as a gift from Prof. Rong from Sun Yat-Sen University and cultured in Dulbecco's Modified Eagle Medium/Nutrient Mixture F-12 (DMEM/F12 1:1; Gibco Life Technologies, USA) supplemented with 5% (v/v) Fetal Bovine Serum and 1% (v/v) Penicillin/Streptomycin. The medium was changed every 2–3 days. All cells were incubated at 37°C in a humidified 5% CO_2 atmosphere.

ATDC5 were seeded on coverslips at a density of 10^4 cells/cm^2. After 24 h in serum-free medium, drug treatment started when the cells reached 60–70% confluence. Working solution was prepared right before use. The final working concentrations of drugs used in this study were as follows: 100 μM hydrogen peroxide (H_2O_2) 100 nM Endothelin-1 (ET-1; Sigma), 1 μM BQ123 (Sigma, USA), 1 μM BQ788 (Sigma, USA), unless specified. Blocker treatment was performed 30 min before H_2O_2 or ET-1 stimulation for 24 h. Various concentrations of vitamin C were added to the cells 1 h before addition of H_2O_2 or ET-1. Technical replicates ($n = 3$–5) were obtained for each assay in subsequent analyses.

Immunostaining was performed on the cells using the antibodies described above. Cells were fixed and permeabilized if deemed necessary. NFκB p65 and $p16^{INK4a}$ was stained to evaluate the H_2O_2- or ET-1-induced inflammation and SnCs accumulation respectively with blockers' pre-treatment.

Evaluation of mitochondrial oxidative stress and dynamics

For measurement of mitochondrial superoxide, 5 μM MitoSOX™ Red mitochondrial superoxide indicator (Molecular Probes, Eugene, USA) was applied to cells, incubated for 10 min at 37°C. Signal was visualized by excitation/emission at 510/580 nm. For evaluation of mitochondrial morphology, mitochondria were labelled with 100 nM MitoTracker® Red CMXRos for 30 min at 37°C. Excitation and emission wavelengths are 579 nm and 599 nm respectively. Fixation and mounting with ProLong® Gold antifade reagent with 4', 6-diamidino-2-phenylindole (DAPI) were performed in these two types of staining. Images were captured using Leica TCS SPE Confocal Microscope (Leica, Mainz, Germany) at a magnification of 630×. ImageJ was used to quantitatively measure the signal intensity and length of mitochondria.

Statistical analysis

All data were presented as mean ± S.E.M, with the mean difference with 95% confidence interval (CI) given in the result. The comparisons of signal intensities and histomorphometric data among different groups were performed using one-way analysis of variance (ANOVA) or Kruskal–Wallis test when deemed appropriate. Respective post-hoc tests were carried when overall significance was detected between groups. Correlation between plasma ET-1 and modified OARSI score (cartilage degradation) was assessed by using Spearman's correlation. Two-tailed Student's *t*-test (unpaired) was performed for comparison between WT and TET-1. The level of significance was set at $p < 0.05$. Analyses and graphs were generated using Prism 8 (GraphPad).

Results

Plasma ET-1 positively correlated with articular cartilage damage in murine PTOA

DMM surgery was performed to generate a post-traumatic murine OA model. From H&E and safranin O/fast green staining, 4-month post-DMM surgery caused disruption of articular surface and proteoglycan loss [Fig. 1(a)]. Thickness of HC decreased substantially from 183.3 ± 11.05 μm in baseline to 77.73 ± 15.02 μm in 4-month post-DMM group [Mean difference (MD) = 105.6, 95%CI (21.76–189.4)] [Fig. 1(b)]. More severe OA developed after 4-month of surgery as demonstrated by assessment of the modified OARSI score (cartilage) by two independent observers [Kappa = 0.735; 95%CI (0.472–0.999)] [Fig. 1(c)].

To study the expression of ET-1 with OA development, local and systemic ET-1 was evaluated using immunostaining and ELISA respectively. With increasing severity of OA, ET-1 expression increased in subchondral bone and synovium but decreased in articular cartilage [Fig. 1(d)]. Plasma ET-1 was found to increase significantly from 3.18 ± 0.21 pg/ml at baseline to 6.47 ± 0.34 pg/ml at 4-month post-DMM [-3.289, 95%CI (−4.771 to −1.807)] [Fig. 1(e)]. A moderate positive relationship [$r^2 = 0.64$, 95%CI (0.349–0.9510)] was observed between the modified OARSI score

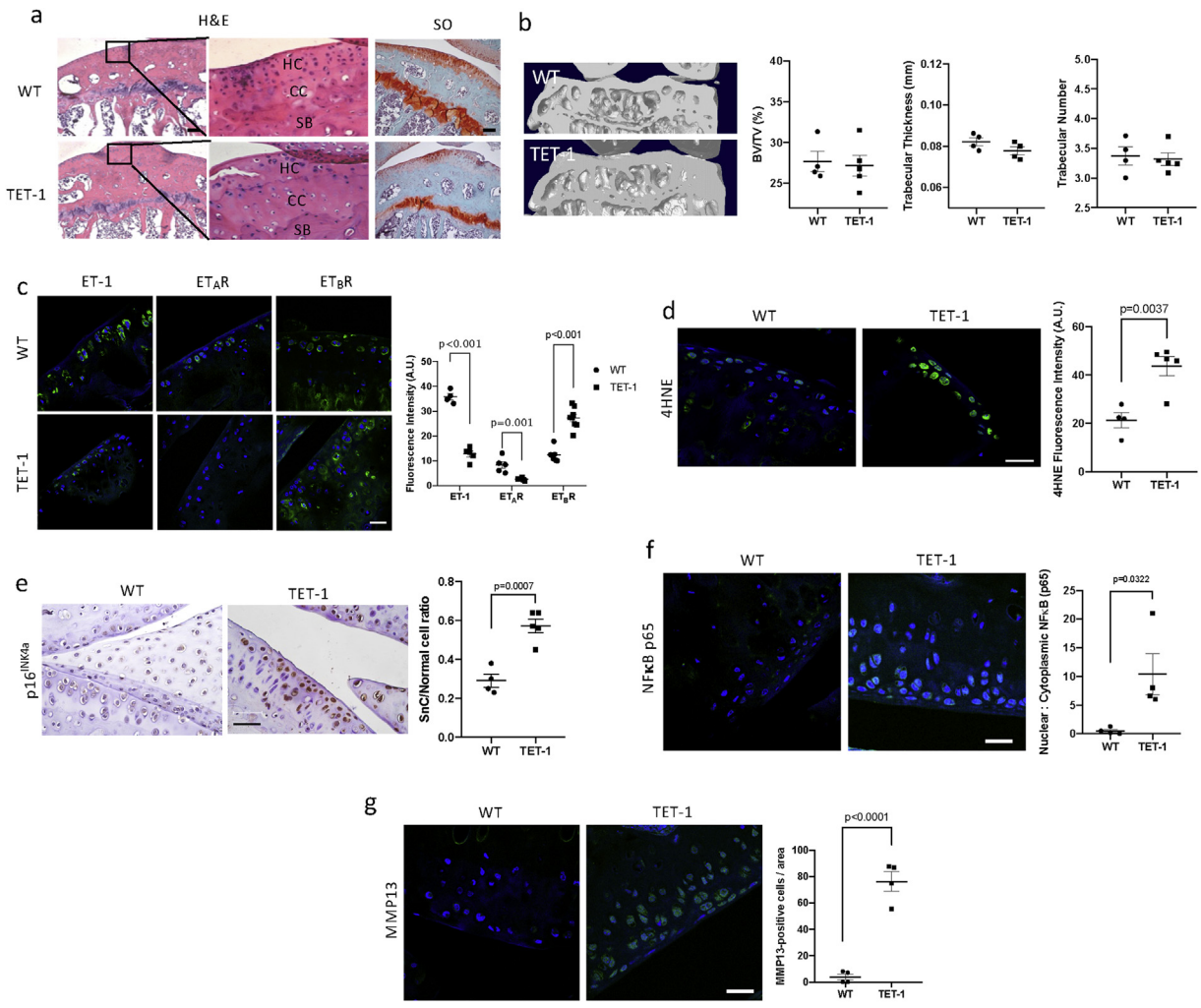

Fig. 2

Transgenic mouse overexpressing ET-1 in endothelial cells displayed OA-like phenotypes and caused chondrocyte senescence (a) Representative images of H&E and Safranin O/Fast green (SO) staining from wildtype (WT) (***n*** = 4) and TET-1 (***n*** = 5) mice. Enlarged images were shown to display close-up views of articular cartilage. HC = hyaline cartilage, CC = calcified cartilage, SB = subchondral bone. Scale bar, 100 μm. (b) Representative images of micro-CT analysis of tibia subchondral bone and its respective BV/TV (%), trabecular thickness and number. (c–d) Representative images of immunofluorescence staining and quantification of (c) ET-1 (green), endothelin receptors, ET_AR (green), ET_BR (green) and (d) 4HNE (green) on articular cartilage of WT and TET-1 mice. (e) Representative images and quantification of immunostaining for $p16^{INK4a}$ (brown) on articular cartilage of WT and TET-1 mice. (f–g) Representative images of immunofluorescence staining and quantification of (f) NFκB p65 (green) and (g) MMP13 (green) on articular cartilage from each group. Scale bar, 25 μm. All data are expressed as means ± SEM, and each data point represents an individual mouse. Two-tailed ***t***-test (unpaired) was performed for statistical analysis.

Osteoarthritis and Cartilage

(cartilage) and plasma ET-1 level, indicating ET-1 positively related to OA severity [Fig. 1(f)].

For receptors expression, we observed alteration of endothelin receptors expression prior to cartilage damage. Before cartilage damage at 1-month post-DMM, ET_AR expression decreased [22.91, 95%CI (8.723–37.1)] while ET_BR expression increased [-30.50, 95%CI (−43.77 to −17.23)] when compared to baseline. After cartilage damage at 4-month post-DMM, expression of ET_AR remained at a low level while ET_BR dropped significantly [59.12, 95%CI (45.85–72.39)] [Fig. 1(g)].

Oxidative stress and senescent chondrocytes (SnCs) accumulation with OA development

Oxidative damage and chondrocytes senescence, as indicated by 4HNE and $p16^{INK4a}$ respectively, increased with the progression of PTOA. Similar to ET_BR, most of the 4HNE- or $p16^{INK4a}$-positive chondrocytes were located on the superficial layer of articular cartilage [Fig. 1(h)]. Increase of 4HNE [-7.09, 95%CI (−13.53 to −0.64)] and $p16^{INK4a}$ [−17.29, 95%CI (−23.01 to −11.58)] expression in cartilage were observed from 1-month post-DMM

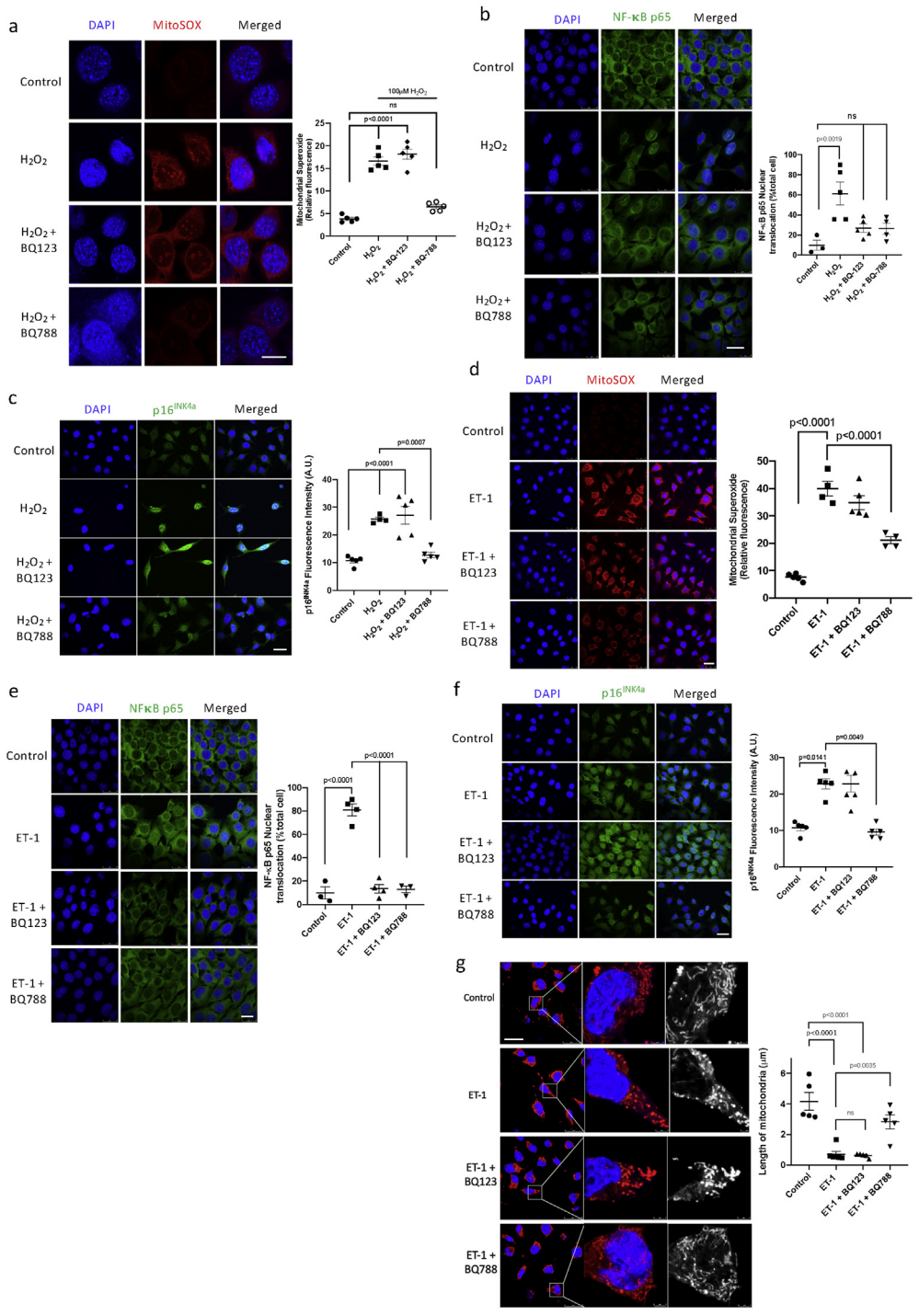

Fig. 3

H_2O_2 or ET-1-induced ROS upregulation and ATDC5 senescence. ATDC5 were grown on coverslips. (a) Representative images and quantification of mitochondrial superoxide production (red) by MitoSOX staining. Cells were treated with vehicle control, 100 μM H_2O_2 or blocker together with H_2O_2. Blockers were added 30 min before H_2O_2 stimulation for 24 h. Scale bar, 10 μm (b–c) Representative images and quantification of (b) NFκB p65 (green) and (c) $p16^{INK4a}$ (green) under different blockers pretreatment. (d) Representative images and quantification of mitochondrial superoxide production (red). Cells were treated with vehicle control, 100 nM ET-1 or blocker together with ET-1. Blockers were added 30 min before ET-1 stimulation for 24 h. (e–f) Representative images and quantification of (e) NFκB p65 (green) and (f) $p16^{INK4a}$ (green) under different blockers pretreatment. (g) Representative images showing mitochondrial morphology and quantitative data of the length of mitochondria. Middle panel shows the enlarged view of a single cell. Right panel shows monochrome images for easier visualization. Scale bar, 25 μm unless specified. Cells were counter-stained with DAPI (blue). All data are expressed as means ± SEM. One-way ANOVA with Tukey's multiple-comparisons test was used for statistical analysis.

Osteoarthritis and Cartilage

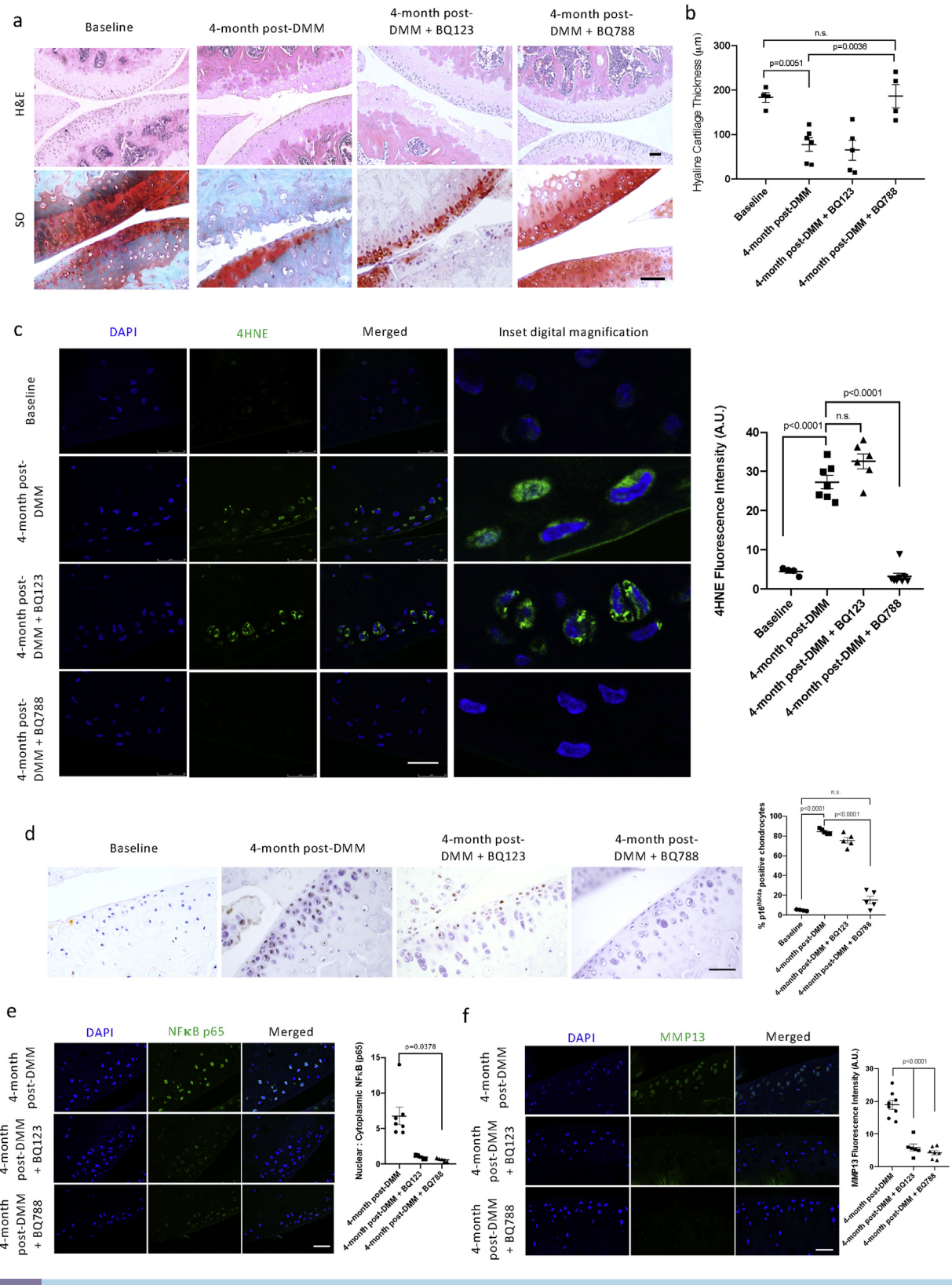

Fig. 4

Selective ET_BR blocker alleviated OA-like cartilage phenotype by lowering ROS and SnCs accumulation. (a) Representative images of H&E and safranin O/Fast green (SO) staining from baseline (***n*** = 4), 4-month post-DMM without drug treatment (***n*** = 7), 4-month post-DMM with BQ123 treatment (***n*** = 8) and 4-month post-DMM with BQ788 treatment (***n*** = 7) mice. Scaler bar, 100 μm. (b) Thickness of hyaline cartilage for each group (c) Representative images of immunofluorescence staining and quantification of 4HNE (green) for

Osteoarthritis and Cartilage

each group with DAPI (blue). Scale bar, 25 μm. Inset digital magnification showing a close-up view of chondrocytes on articular cartilage. (d) Representative images and quantification of immunostaining for $p16^{INK4a}$ (brown) on articular cartilage for each group. Scale bar, 50 μm (e–f) Representative images of immunofluorescence staining and quantification of (e) NFκB p65 (green) and (f) MMP13 (green) on articular cartilage from each group. Scale bar, 25 μm. All data are expressed as means ± SEM, and each data point represents an individual mouse. One-way ANOVA with Tukey's multiple-comparisons test was used for statistical analysis.

onwards together with the upregulation of ET_BR. Similarly, we observed an increased in NFκB p65 translocation from cytoplasm to nucleus [-6.471, 95%CI (−12.69 to −0.2473)] [Fig. 1(i)] and MMP13 production [-13.34, 95%CI (−21.49 to −5.183)] [Fig. 1(j)] starting from 1-month after DMM surgery.

Overexpressed endothelial ET-1 led to SnCs accumulation and articular cartilage damage

A transgenic mouse model overexpressing ET-1 in endothelial cells (TET-1) was used to study the effect of ET-1 in OA pathogenesis. It was reported that TET-1 developed OA phenotypes at the age of 9-month. Damage of HC, thickening of calcified cartilage (CC) and loss of proteoglycan were observed in 9-month TET-1 mice when compared to wildtype (WT) littermates using H&E and safranin O/fast green staining [Fig. 2(a)]. However, no significant changes were observed in tibial subchondral bone plate [Fig. 2(b)]. Fewer ET-1 and ET_AR but more ET_BR expression were found at articular cartilage of TET-1 mice [Fig. 2(c)], with a trend similar to OA cartilage in DMM model. Similar to DMM-induced OA cartilage, TET-1 cartilage showed a significant increase in 4HNE [22.38, 95%CI (9.955–34.80)] and $p16^{INK4a}$ expression [0.2820, 95%CI (0.1656–0.3984)] [Fig. 2(d) and (e)], showing high level of oxidative stress and senescent cells at cartilage when ET-1 is overexpressed. TET-1 mice also displayed significantly more NFκB translocation [9.907, 95%CI (1.174–18.64)] and MMP13 production [72.36, 95%CI (53.35–91.36)] at articular cartilage than WT animals [Fig. 2(f) and (g)].

H_2O_2 or ET-1-induced ROS accumulation and chondrocyte senescence via ET_BR in vitro

ATDC5 treated with 100 μM H_2O_2 for 24 h showed an increase of mitochondrial superoxide [−12.76, 95%CI (−15.72 to −9.794)] compared to control group. Thirty minutes pre-treatment of BQ788 but not BQ123, inhibited the increase [10.09, 95%CI (6.641–13.54)] [Fig. 3(a)]. Immunostaining of NFκB p65 and $p16^{INK4a}$ showed that both endothelin receptor blockers could reduce the nuclear translocation of NFκB p65, while only BQ788 could reduce H_2O_2-induced chondrocyte senescence [12.92, 95%CI (4.066–21.77)] [Fig. 3(b) and (c)].

Similar to H_2O_2, 100 nM ET-1 stimulated production of mitochondrial oxidative stress in ATDC5 after 24 h of incubation, Again, pretreatment of BQ788 but not BQ123 prevented oxidative stress accumulation in mitochondria [18.89, 95%CI (10.44–27.33)] [Fig. 3(d)]. ET-1 also promoted NFκB p65 translocation and $p16^{INK4a}$ accumulation [Fig. 3(e) and (f)]. Similar to the observations *in vivo*, both selective blockers decreased NFκB p65 translocation from cytoplasm to nucleus, indicating endothelin receptors blockade suppressed ET-1-induced NFκB activation [Fig. 3(e)]. Senescent cells accumulation was also lowered by selective ET_BR blockade [13.16, 95%CI (2.625–23.7)] [Fig. 3(f)], suggesting ET-1 causes increase of ROS and senescent cells possibly through ET_BR. ET-1 also caused changes in mitochondria morphology from tubular to blob form, this indicates the stress caused by ET-1 to the cells can be reflected by shape change of mitochondria. ET-1 also reduced the length of mitochondria from ~4 μm to ~0.6 μm. Blocking ET_BR selectively restored ET-1-induced change in mitochondrial dynamics and increased the length of mitochondria [Fig. 3(g)].

Selective blockade of ET_BR, but not ET_AR could lower ROS, mitigate chondrocyte senescence and articular cartilage in vivo

To investigate the effect of drugs *in vivo*, BQ123 or BQ788 was intraperitoneally injected to DMM mice. Our result showed that ET_BR but not ET_AR antagonism rescued cartilage degradation and proteoglycan loss after 4-month of DMM surgery [Fig. 4(a)]. Thickness of HC in BQ788-treated group was restored to a level (186.4 ± 26.24 μm) that is insignificant to baseline (183.3 ± 11.05 μm) [Fig. 4(b)]. Only BQ788 but not BQ123 lowered 4HNE [24.17, 95%CI (18.94–29.39)] and $p16^{INK4a}$ expression [69.19, 95%CI (57.81–80.57)] [Fig. 4(c) and (d)], indicating an important link between ET_BR, oxidative stress accumulation and chondrocyte senescence. However, both selective receptor blockers reduced NFκB p65 translocation and MMP13 production (Fig, 4(e)-(f)). These findings indicated selective blockade of endothelin type B receptor rescued OA cartilage phenotypes possibly through reduction of oxidative stress and senescence accumulation in chondrocytes. While NFκB may play a role in ET-1-induced MMP13 increase via both endothelin receptors.

Endothelin receptor antagonism improves DMM-induced subchondral bone changes and synovial vessels function

Micro-CT analysis of DMM tibia subchondral bone showed osteophytes formation and thickening of tibial plateau with reduction in trabecular number and increase in trabecular thickness compared to baseline. Both BQ123 and BQ788 treatment reversed DMM-induced changes of tibia subchondral bone plate [Fig. 5(a)–(d)], suggesting blocking either one of the endothelin receptors could rescue osteoarthritic changes of subchondral trabecular bone. Using PD and photoacoustic imaging techniques reported by our group previously[11], we demonstrated better synovial vascular function, reduced synovial angiogenesis and higher tissue oxygenation level in OA knee after endothelin receptor blockers treatment [Fig. 5(e)]. Besides, histological analysis showed a reduction of blood vessels per area in synovium after 1-month of blockers treatment [Fig. 5(f)], which further confirms endothelin receptors play a role in endothelial dysfunction.

ET-1 induced chondrocytes senescence through ROS accumulation

To elucidate the causal relationship between ROS accumulation and ET-1-induced chondrocyte senescence, different concentrations of vitamin C (Vit C), a typical ROS scavenger, were added to the

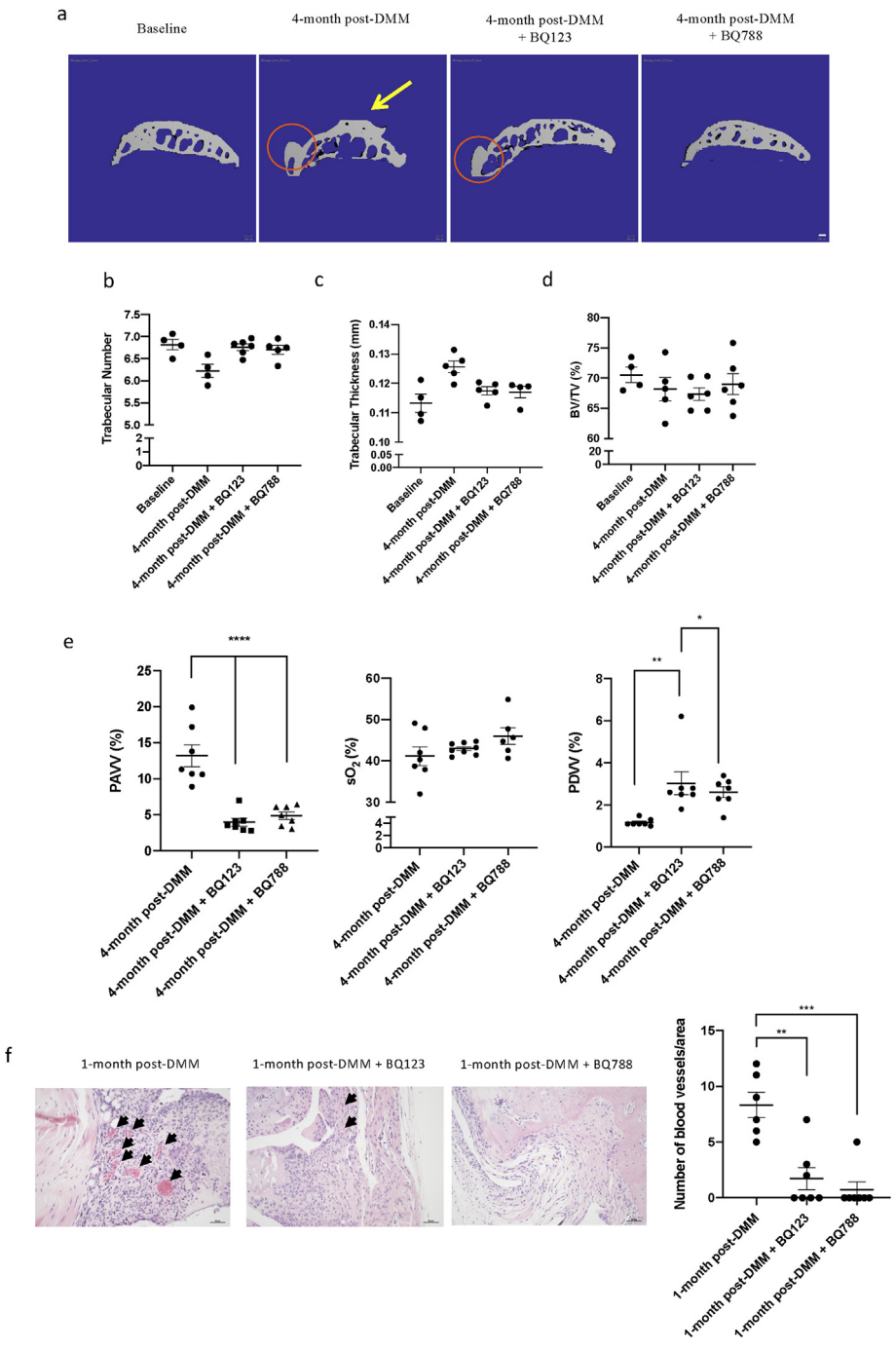

Fig. 5

Endothelial dysfunction in synovium and changes in tibial subchondral bone of DMM mice could be rescued by endothelin receptor blockers. (a–d) Representative images and quantification of micro-CT analysis of tibial subchondral bone under different blockers treatment. Yellow arrow indicates thickening of tibial plateau and red circles indicate osteocyte formation. Scale bar, 100 μm. (b) Trabecular number (c) thickness and (d) BV/TV (%) showed no significance between groups. (e) Vascular volume derived from photoacoustic signal (PAVV), percentage of oxygen saturation (sO_2) and vascular volume derived from power doppler signal (PDVV) were shown. Result indicated less synovial angiogenesis, higher tissue oxygenation level and increased vascularity function in synovium after endothelin receptor blockers treatment. (f) Representative images and quantification of blood vessels in synovium of DMM-knees using H&E staining. Newly formed blood vessels (black arrows) were found after 1-month of DMM surgery. Blockers treatments significantly lowered the number of blood vessels. Scale bar, 50 μm. All data are expressed as means ± SEM, and each data point represents an individual mouse.

Osteoarthritis and Cartilage

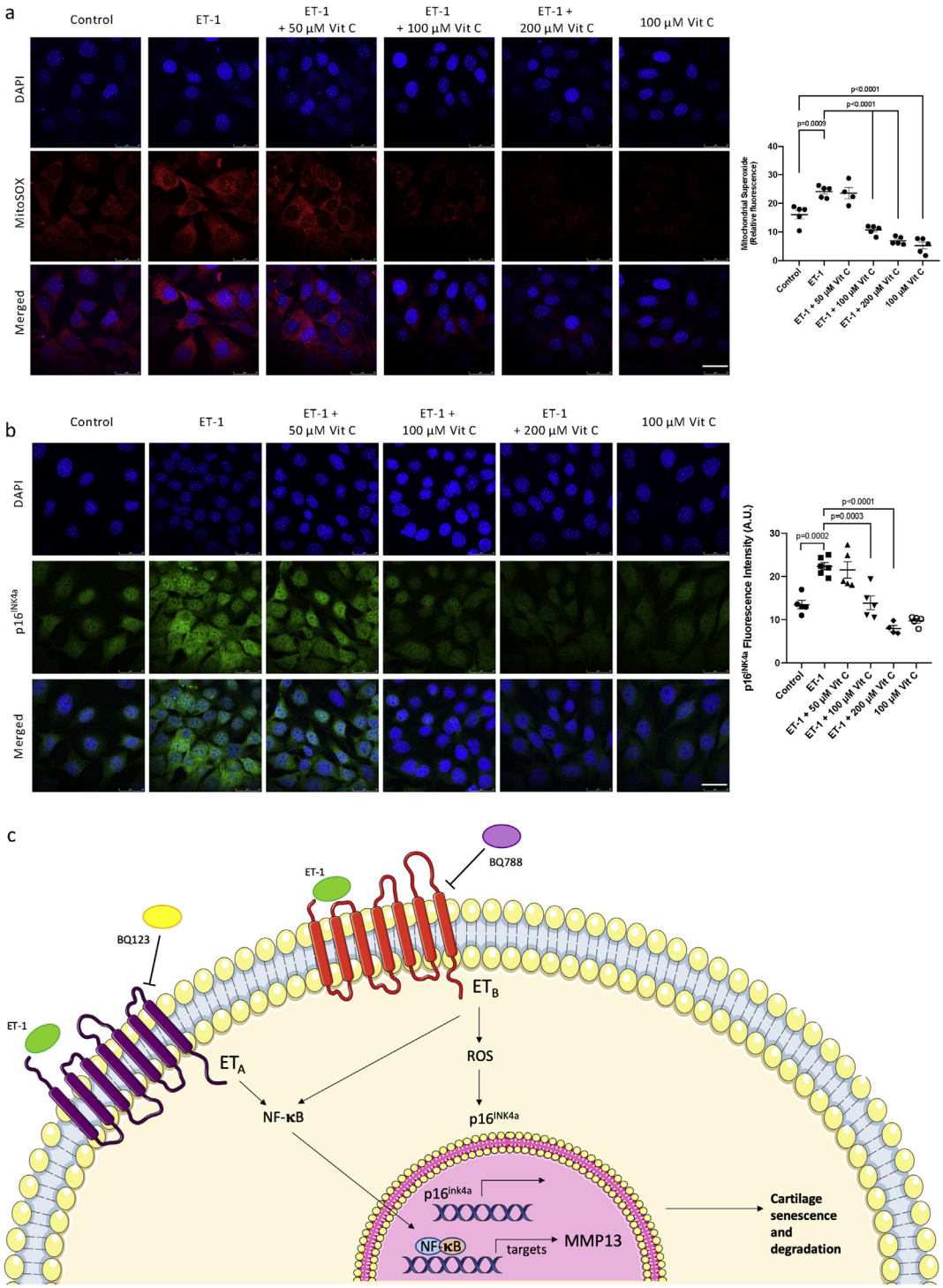

Fig. 6

ROS is an upstream of ET-1-induced p16^{INK4a} (a–b) Representative images and quantification of (a) mitochondrial superoxide (red) and (b) p16^{INK4a} (green) in ATDC5 stimulated by ET-1 with various concentrations of vitamin C pretreatment. Vitamin C was incubated with the cells for 1 h before ET-1 treatment for 24 h. Scale bar, 25 μm. All data are expressed as means ± SEM. One-way ANOVA with Tukey's multiple-comparisons test was used for statistical analysis. (c) A schematic diagram showing the proposed mechanism of ET-1 induced cartilage senescence and degradation in PTOA.

Osteoarthritis and Cartilage

cells 1 h before ET-1 stimulation. We found that 100 μM or higher concentration of vitamin C significantly lowered ET-1-induced mitochondrial superoxide by more than half [100 μM Vit C: 13.41, 95%CI (8.27–18.55); 200 μM: 17.18, 95%CI (12.04–22.32)] [Fig. 6(a)]. The same concentration, i.e., 100 μM of vitamin C, also reduced senescence maker $p16^{INK4a}$ by half [100 μM Vit C: 8.519, 95%CI (3.454–13.58); 200 μM: 14.43, 95%CI (9.035–19.83)] [Fig. 6(b)]. This implicated ET-1-induced chondrocyte senescence could be reduced by removing oxidative stress in cells. We inferred that ET-1-induced chondrocyte senescence occurs via ROS accumulation.

Discussion

Endothelium-derived ET-1 induces not only cellular senescence in blood vessels but also in bone and joint. Firstly, our data showed that both H_2O_2 and ET-1 led to accumulation of oxidative stress and chondrocyte senescence *in vitro*. Secondly, we demonstrated ET-1 induced chondrocyte senescence through accumulation of ROS via ET_BR but not ET_AR. Thirdly, ET_BR is responsible for replicative senescence and SASPs production that lead to cartilage damage in OA development, while ET_AR is responsible for SASPs production only [Fig. 6(C)]. Fourthly, selective blockade of ET_BR successfully alleviated OA-like cartilage changes in a PTOA murine model, indicating cartilage damage on OA development is more likely to be driven by replicative senescence via ET_BR but not SASPs production via ET_AR. For the first time, a direct effect of endothelial dysfunction and the role of endothelin type B receptor in OA pathogenesis have been reported.

Despite an increase of ET-1 expression in subchondral bone, synovium and plasma with increasing OA severity, expression of ET-1 decreased in articular cartilage. Intriguingly, we observed an upregulation of ET_BR in cartilage when OA develops. ET_BR, has been known as a clearance receptor to remove excess ET-1[24]. Angiogenesis in synovium and subchondral bone was reported in OA knee joints in some of our previous studies[10,11]. This is a possible explanation why ET-1 is highly expressed in these highly vascularized structure instead of avascular articular cartilage in OA joints. Due to the abundance of blood vessels in these structures, the increase of ET_BR may not be sufficient to clear away the excess ET-1 secreted by the endothelial cells. This explains the tissue-specific property of ET-1 expression within a joint.

Given overexpression of ET-1 leads to OA phenotypes, blocking endothelin receptors to prevent transduction of ET-1 via ET_AR or ET_BR would be a possible way to alleviate OA symptoms. A study showed improvement in radiographic indices of OA after treating ACLT-induced rat with ET_AR blocker BQ123[21]. Their study mainly focused on bone changes and nociceptive tolerance, yet cartilage changes were less studied. In our study, we studied the effect of both selective ET_AR or ET_BR blockade to rescue of OA. However, our results suggested that ET_BR blocker BQ788 but not BQ123 brought genuine protective effect to OA cartilage from injury. The discrepancy in result may due to the different drug administration regimes, weekly injection was used in Kaufman's study while we employed daily injection. The half-life of BQ123 is less than 15 min[25], which raised our concern on the effectiveness of weekly administration of this drug to OA joint. In our study, we observed that ET_AR antagonist lowered NFκB and MMP-13, yet failed to remove SnCs and preserve cartilage integrity in OA joint. It indicates that it is not sufficient to rescue OA by only targeting SASPs. Together with unsatisfactory results from a variety of clinical trials on IL-1β, IL-6[26,27], our work implies that replicative senescence of chondrocytes might contribute more to OA pathology compared to SASPs.

However, the role of replicative senescence of chondrocytes in OA pathology remains controversial. A recent study by Jeon and colleagues showed local clearance of $p16^{INK4a}$-positive cells at articular joint attenuated cartilage damage in a PTOA model[6]. However, the other study showed conflicting results that conditioned knockout of $p16^{INK4a}$ in aggrecan-positive cells, i.e., chondrocytes, failed to alleviate cartilage damage and joint destruction after DMM[28]. Our findings well aligned with Jeon's findings. Moreover, our pharmaceutical treatment not only removed senescent cells in articular cartilage but also in subchondral bone (Fig. S3). It indicates that it is critical to remove senescent cells from whole joint tissues, rather than simply eliminating them from articular cartilage for rescue of OA.

A few limitations of the study should be noted. Firstly, OA is a whole joint disease, not limited to articular cartilage. We suggested removal of senescent cells from the whole joint can alleviate PTOA. In this study, we focused on the direct effect of endothelial dysfunction on cartilage, with only some changes in synovium reported. Our results suggest endothelin receptor blockers can rescue endothelial dysfunction in both cartilage and synovium, driving removal of senescent cells. Further investigation is needed to confirm our postulation. Secondly, we reported the effect of two selective endothelin receptor blockers to cartilage damage but the effect of dual receptors blocker was not included. Both selective endothelin receptor blockers led to reduction of MMP13, which is a major SASP causing OA progression. Bosentan, a dual endothelin receptor blocker, lowered the increase of p16 and SA-β-Gal expression in endothelial cells[15]. In future, we will investigate the effect of dual receptors blockade on rescue of OA.

To our best knowledge, we for the first time, decipher the molecular basis of endothelial dysfunction, i.e., ET-1/ET_BR signalling, in the pathogenesis and management of PTOA. It provides us a new insight into the vascular aetiology of OA and opens a door for mechanism-based discovery for disease-modifying OA drugs targeting endothelial dysfunction. In the past decade, the focus of our research was placed on the bone-cartilage crosstalk; the findings generated from the present study highlight the importance of synovial angiogenesis in chondrocyte senescence and cartilage damage. Apart from the structural damage, our work warrants further investigation into the role of ET-1/ET_BR in synovitis and OA pain.

Author contributions

MTA, ZYL and CYW designed the study. MTA and ZYL performed experiments and analysed data. MTA performed all the staining and *in vitro* study. ZYL performed the surgery, contributed to ultrasound imaging data collection, measured plasma ET-1 concentration and evaluated severity of OA. YPZ contributed to ultrasound imaging data collection, 3D data analysis and interpretation. LMR contributed to study design and data interpretation from clinical perspective. MTA prepared the draft of the manuscript, which was revised by CYW. All authors have read and approved the final version of the manuscript.

Competing interest statement

We declare that there are no conflicts of interest.

Role of funding source

This work was supported by Research Grants Council of Hong Kong Early Career Scheme (PolyU 251008/18M), PROCORE-France/Hong Kong Joint Research Scheme (F-PolyU504/18) and also Health and Medical Research Fund Scheme (01150087#, 15161391#, 16172691#). The study funders/study sponsors had no involvement in the study design, data collection, analysis or interpretation of the study, or in the writing of, or decision to submit the manuscript.

Acknowledgements

The authors wish to thank University Research Facility in Life Sciences (ULS) for providing equipment and technical support. The authors would also like to thank Boris Chan and Billy Yang for their contribution to characterization of TET-1 mice in this project.

Supplementary data

Supplementary data to this article can be found online at https://doi.org/10.1016/j.joca.2020.08.006.

References

1. Lawrence RC, Felson DT, Helmick CG, Arnold LM, Choi H, Deyo RA, *et al*. Estimates of the prevalence of arthritis and other rheumatic conditions in the United States. Part II. Arthritis Rheum 2008;58(1):26–35, https://doi.org/10.1002/art.23176.
2. Price JS, Waters JG, Darrah C, Pennington C, Edwards DR, Donell ST, *et al*. The role of chondrocyte senescence in osteoarthritis. Aging Cell 2002;1(1):57–65.
3. Harbo M, Delaisse JM, Kjaersgaard-Andersen P, Soerensen FB, Koelvraa S, Bendix L. The relationship between ultra-short telomeres, aging of articular cartilage and the development of human hip osteoarthritis. Mech Ageing Dev 2013;134(9):367–72, https://doi.org/10.1016/j.mad.2013.07.002.
4. Harbo M, Bendix L, Bay-Jensen AC, Graakjaer J, Soe K, Andersen TL, *et al*. The distribution pattern of critically short telomeres in human osteoarthritic knees. Arthritis Res Ther 2012;14(1), https://doi.org/10.1186/ar3687. R12.
5. Yudoh K, Nguyen v T, Nakamura H, Hongo-Masuko K, Kato T, Nishioka K. Potential involvement of oxidative stress in cartilage senescence and development of osteoarthritis: oxidative stress induces chondrocyte telomere instability and down-regulation of chondrocyte function. Arthritis Res Ther 2005;7(2):R380–91, https://doi.org/10.1186/ar1499.
6. Jeon OH, Kim C, Laberge RM, Demaria M, Rathod S, Vasserot AP, *et al*. Local clearance of senescent cells attenuates the development of post-traumatic osteoarthritis and creates a pro-regenerative environment. Nat Med 2017;23(6):775–81, https://doi.org/10.1038/nm.4324.
7. Philipot D, Guerit D, Platano D, Chuchana P, Olivotto E, Espinoza F, *et al*. p16INK4a and its regulator miR-24 link senescence and chondrocyte terminal differentiation-associated matrix remodeling in osteoarthritis. Arthritis Res Ther 2014;16(1):R58, https://doi.org/10.1186/ar4494.
8. Findlay DM. Vascular pathology and osteoarthritis. Rheumatology 2007;46(12):1763–8, https://doi.org/10.1093/rheumatology/kem191 (Oxford).
9. Mapp PI, Walsh DA. Mechanisms and targets of angiogenesis and nerve growth in osteoarthritis. Nat Rev Rheumatol 2012;8(7):390–8, https://doi.org/10.1038/nrrheum.2012.80.
10. Zhen G, Wen C, Jia X, Li Y, Crane JL, Mears SC, *et al*. Inhibition of TGF-beta signaling in mesenchymal stem cells of subchondral bone attenuates osteoarthritis. Nat Med 2013;19(6):704–12, https://doi.org/10.1038/nm.3143.
11. Liu Z, Au M, Wang X, Chan P-MB, Lai P, Sun L, *et al*. Photoacoustic imaging of synovial tissue hypoxia in experimental post-traumatic osteoarthritis. Prog Biophys Mol Biol 2018, https://doi.org/10.1016/j.pbiomolbio.2018.03.009.
12. Barton M. Aging and endothelin: determinants of disease. Life Sci 2014;118(2):97–109, https://doi.org/10.1016/j.lfs.2014.09.009.
13. Sin A, Tang W, Wen CY, Chung SK, Chiu KY. The emerging role of endothelin-1 in the pathogenesis of subchondral bone disturbance and osteoarthritis. Osteoarthritis Cartilage 2015;23(4):516–24, https://doi.org/10.1016/j.joca.2014.11.002. /OARS, Osteoarthritis Research Society.
14. Dong F, Zhang X, Wold LE, Ren Q, Zhang Z, Ren J. Endothelin-1 enhances oxidative stress, cell proliferation and reduces apoptosis in human umbilical vein endothelial cells: role of ETB receptor, NADPH oxidase and caveolin-1. Br J Pharmacol 2005;145(3):323–33, https://doi.org/10.1038/sj.bjp.0706193.
15. Olmos G, Martinez-Miguel P, Alcalde-Estevez E, Medrano D, Sosa P, Rodriguez-Manas L, *et al*. Hyperphosphatemia induces senescence in human endothelial cells by increasing endothelin-1 production. Aging Cell 2017;16(6):1300–12, https://doi.org/10.1111/acel.12664.
16. Zhao Z, Li E, Cao Q, Sun J, Ma B. Endothelin-1 concentrations are correlated with the severity of knee osteoarthritis. J Invest Med 2016;64(4):872–4, https://doi.org/10.1136/jim-2015-000030.
17. Wilson SH, Simari RD, Lerman A. The effect of endothelin-1 on nuclear factor kappa B in macrophages. Biochem Biophys Res Commun 2001;286(5):968–72, https://doi.org/10.1006/bbrc.2001.5485.
18. Wu MH, Lo JF, Kuo CH, Lin JA, Lin YM, Chen LM, *et al*. Endothelin-1 promotes MMP-13 production and migration in human chondrosarcoma cells through FAK/PI3K/Akt/mTOR pathways. J Cell Physiol 2012;227(8):3016–26, https://doi.org/10.1002/jcp.23043.
19. Salminen A, Kauppinen A, Kaarniranta K. Emerging role of NF-kappaB signaling in the induction of senescence-associated secretory phenotype (SASP). Cell Signal 2012;24(4):835–45, https://doi.org/10.1016/j.cellsig.2011.12.006.
20. Glasson SS, Blanchet TJ, Morris EA. The surgical destabilization of the medial meniscus (DMM) model of osteoarthritis in the 129/SvEv mouse. Osteoarthritis Cartilage 2007;15(9):1061–9, https://doi.org/10.1016/j.joca.2007.03.006.
21. Kaufman GN, Zaouter C, Valteau B, Sirois P, Moldovan F. Nociceptive tolerance is improved by bradykinin receptor B1 antagonism and joint morphology is protected by both endothelin type A and bradykinin receptor B1 antagonism in a surgical model of osteoarthritis. Arthritis Res Ther 2011;13(3):R76, https://doi.org/10.1186/ar3338.
22. Pritzker KP, Gay S, Jimenez SA, Ostergaard K, Pelletier JP, Revell PA, *et al*. Osteoarthritis cartilage histopathology: grading and staging. Osteoarthritis Cartilage 2006;14(1):13–29, https://doi.org/10.1016/j.joca.2005.07.014. /OARS, Osteoarthritis Research Society.
23. Kamekura S, Hoshi K, Shimoaka T, Chung U, Chikuda H, Yamada T, *et al*. Osteoarthritis development in novel experimental mouse models induced by knee joint instability. Osteoarthritis Cartilage 2005;13(7):632–41, https://doi.org/10.1016/j.joca.2005.03.004. /OARS, Osteoarthritis Research Society.
24. Schneider MP, Boesen EI, Pollock DM. Contrasting actions of endothelin ET(A) and ET(B) receptors in cardiovascular disease. Annu Rev Pharmacol Toxicol 2007;47:731–59, https://doi.org/10.1146/annurev.pharmtox.47.120505.105134.
25. Shin H-c. Pharmacokinetics of endothelin antagonist BQ-123 in rats and Guinea pigs. Kor J Lab Anin Sci 2000;16(1):1–8.
26. Fleischmann RM, Bliddal H, Blanco FJ, Schnitzer TJ, Peterfy C, Chen S, *et al*. A phase II trial of Lutikizumab, an anti-interleukin-1alpha/beta dual variable domain immunoglobulin, in knee osteoarthritis patients with synovitis. Arthritis Rheumatol 2019;71(7):1056–69, https://doi.org/10.1002/art.40840.
27. Chevalier X, Goupille P, Beaulieu AD, Burch FX, Bensen WG, Conrozier T, *et al*. Intraarticular injection of anakinra in osteoarthritis of the knee: a multicenter, randomized, double-

blind, placebo-controlled study. Arthritis Rheum 2009;61(3): 344–52, https://doi.org/10.1002/art.24096.
28. Diekman BO, Sessions GA, Collins JA, Knecht AK, Strum SL, Mitin NK, *et al*. Expression of p16(INK) (4a) is a biomarker of chondrocyte aging but does not cause osteoarthritis. Aging Cell 2018;17(4), https://doi.org/10.1111/acel.12771. e12771.